Macromolecules

Article

pubs.acs.org/Macromolecules

Molecular Mobility and Glass Transition of Thin Films of Poly(bisphenol A carbonate)

Huajie Yin,[†] Simone Napolitano,[‡] and Andreas Schönhals*,[†]

[†]BAM Federal Institute for Materials Research and Testing, Unter den Eichen 87, D-12200 Berlin, Germany

[‡]Department of Physics, Université Libre de Bruxelles, Boulevard du Triomphe CP 223, Bâtiment NO, B-1050 Bruxelles, Belgium

ABSTRACT: Glass transition behavior of thin poly(bisphenol A carbonate) (PBAC) films capped between two aluminum (Al) layers is investigated by means of dielectric expansion dilatometry and dielectric relaxation spectroscopy accompanied by contact angle measurements. The thermal glass transition temperature is more or less independent of the film thickness down to 20 nm. For thickness below 20 nm, an increase of T_g is observed. Meanwhile, an increase of the relaxation time at a fixed temperature is observed for the film with the thickness of 19 nm on the basis of a careful analysis of the temperature dependence of the relaxation rates. A more detailed analysis of the relaxation map reveals that the Vogel temperature increases and the fragility decreases systematically with decreasing film thickness. These properties are discussed in terms of the formation of a boundary layer with PBAC segments adsorbed onto the Al electrode due to the strong interaction between the Al and PBAC layers (2.51 mJ/m^2), which results in a reduced molecular mobility with regard to bulk PBAC behavior. As the dielectric strength is proportional to the number of segments fluctuating on the time and length scale of the dynamic glass transition, it is used as a unique probe of the deviations from bulk behavior. The temperature dependence of the penetration depth of the interfacial interactions on the structural relaxation is further quantitatively determined. The dynamic length scale of the perturbations into the chain conformations responsible for the deviation from bulk behavior is estimated to be smaller than 9 nm.

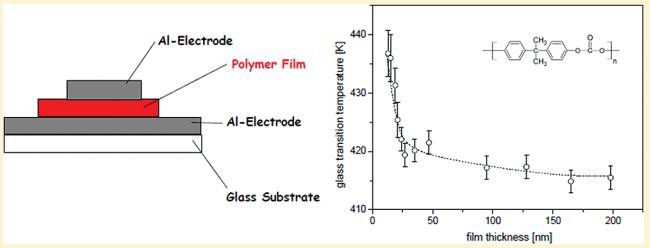

1. INTRODUCTION

Ultrathin polymer films are of considerable technological interest in a wide range of areas ranging from coatings to organic electronic devices. Their properties can be tuned at low production costs. From the scientific point of view, thin polymer films provide an ideal sample geometry for studying the effect of nanometric confinement on the structure and dynamics of polymers. Since the pioneering work of Keddie and Jones on the thickness dependence of the glass transition temperature, T_g,[1] the discussion on polymer dynamics in thin films is in the focus of scientific research and was extended to many other confinement-induced phenomena.[2] When the thickness of a polymer film is smaller than the radius of gyration of the unperturbed polymer chain, such films reveal characteristics strongly deviating from the respective bulk properties in terms of glass transition,[3] viscoelasticity,[4] crystallization kinetics,[5] diffusion,[6] etc. The glass transition of thin polymer films has been investigated for instance by X-ray reflectivity,[7−9] neutron scattering,[10,11]Brillouin light scattering,[12,13] calorimetry,[14−18] ellipsometry,[17−24] various types of fluorescence spectroscopy,[25−28] mechanical spectroscopic techniques,[29,30] positronium lifetime spectroscopy,[31,32] and especially by broadband dielectric spectroscopy.[15,17,33−37] In spite of the large amount of data, a general theory to describe confinement effects on polymer properties has not been developed yet. The question of how a solid interface influences the structure and dynamics of a polymer is still controversially discussed.

Keddie et al. reported a decrease of the glass transition temperature with decreasing film thickness for polystyrene (PS) on both gold and silicon oxide substrates.[1] However, dielectric measurements[38] on thin PS films do not show an obvious dependence of the relaxation rate on the film thickness down to few nanometers as well as the measurements performed via atomic force microscopy (AFM) based shear modulation spectroscopy,[29] ellipsometry,[17] or differential ac-chip calorimetry.[16,39] In the case of polymers like poly(2-vinylpyridine) (P2VP),[40] poly(vinyl chloride) (PVC),[41] polysulfone (PSU),[37] and poly(ethylene terephthalate) (PET),[42] which have rather strong interactions with the substrates (silicon wafers or thermally evaporated Al layers), an increase in T_g upon reduction of the film thicknesses is observed. Also, the dielectric strength, a quantity proportional to the volume fraction of segments participating in the structural relaxation, decreases strongly with decreasing film thickness,[27,42,43] which is interpreted as the effect of a reduced mobility layer.[33,44] Torkelson et al.[45] studied the glass transition behavior of styrene/methyl methacrylate (S/MMA) random copolymer films with varying S-content by intrinsic fluorescence measure-

Received: September 20, 2011
Revised: January 12, 2012
Published: January 30, 2012

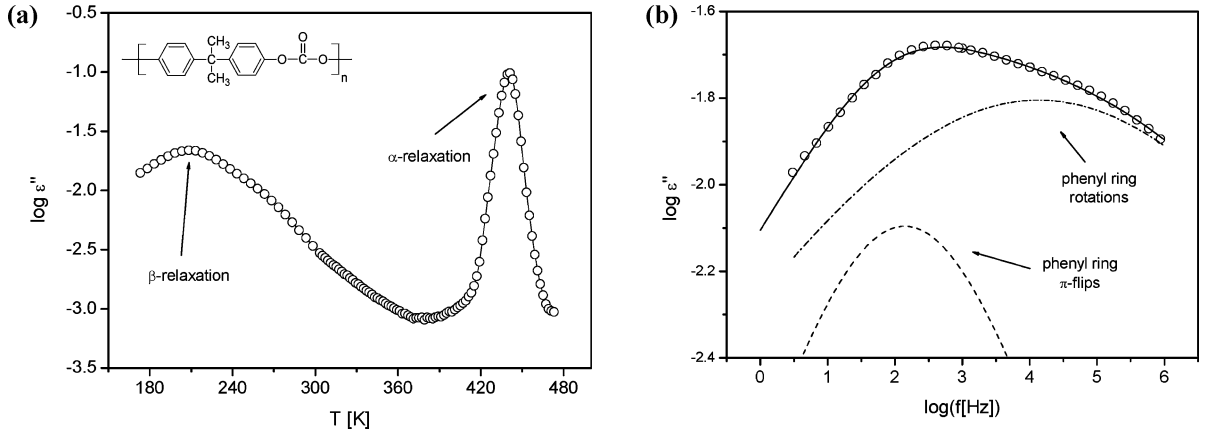

Figure 1. (a) Dielectric loss vs temperature for bulk PBAC at a frequency of 1 kHz. The line is a guide for the eyes. The inset gives the chemical structure of polycarbonate. (b) Dielectric loss versus frequency for the β-relaxation at T = 198.2 K. The solid line is a fit of two HN-functions to the data. The dashed line is the contribution of the π-flips of the phenyl rings, and the dotted-dashed line gives the contributions of the rotations of the phenyl rings.

ments to establish different polymer−substrate interactions. It was found that the glass transition temperature changes from a reduction to an increase of T_g relative to the bulk value as the S-content is reduced from 100 to 22 mol %. Such experimental observations can be discussed in terms of an interplay between confinement and surface effects. The confinement effect makes the glass transition faster compared to the bulk while the surface effect causes a decrease in segmental mobility provided that an attractive interaction of the polymers with the solid substrate is present. The existence of a solid substrate having strong interactions with the polymer film will decrease the configurational space available for the polymer chain to perform transitional motions or Brownian movements. Frictional forces between the polymer and substrate also hinder the segmental movement.[46] Fryer et al.[47] reported a direct correlation between the substrate/polymer interaction, γ_{sp}, and the change of T_g compared to the bulk. For low values of the interfacial energy (γ_{sp} < 2 mJ/m^2), the T_g of the thin polymer films is lower than the corresponding bulk value. For high values of the interfacial energy (γ_{sp} > 2 mJ/m^2), the T_g of the thin polymer films is higher than that of the bulk. On the other hand, it was also pointed out that the polymer−surface interaction energy is not the only parameter which contributes to the thickness dependence of the glass transition temperature. In addition to that, the preparation of the sample, like annealing conditions, may also affect the glass transition temperature.[48,49] Moreover, the density of the segments close to the surface and/or polymer microstructure should be taken into consideration.[50,51]

Although polycarbonate is a commercially important polymer, there are only few investigations with regard to its behavior in ultrathin films. Incoherent neutron scattering measurements were performed on thin supported (Si wafer with a native SiO_2 surface) polycarbonate films by Soles et al.[10,11] At temperatures above T_g the mean-square displacement is strongly reduced compared to the bulk and decreases with decreasing film thickness. Moreover, the localized fluctuations in the glassy state are also increasingly suppressed as the layer thickness decreases. Green et al.[52] studied thin tetramethylbisphenol-A polycarbonate (TMPC) films spin-coated on silicon substrates (with 2 nm native SiO_x layer) by ellipsometric measurement, which revealed that the T_g of TMPC films increases with decreasing film thickness. X-ray reflectivity measurements show a reduction in the glass transition temperature with decreasing film thickness for hydrophilic silicon oxide substrates (ca. −20 K).[53] This is confirmed by positron annihilation lifetime spectroscopy.[54] For hydrophobic passivated silicon substrates T_g is more or less independent of the layer thickness.[53] Torkelson et al. report a T_g reduction with decreasing film thickness by employing fluorescence spectroscopy.[55]

In this contribution, dielectric relaxation spectroscopy is employed to investigate the molecular dynamics of ultrathin polycarbonate films where polycarbonate is capped between aluminum layers in detail. In addition to that, contact angle measurements were employed to confirm the strong interaction energy between aluminum and polycarbonate.

On the basis of the experimental work, it can be concluded that the molecular mobility and glass transition of thin polycarbonate films capped between the aluminum layers show a deviation from the bulk behavior when the film thickness is smaller than 20 nm. Such deviation is caused by the formation of an interface layer with a reduced molecular mobility due to the strong interaction between polycarbonate and aluminum layers. The nonlinear reduction of the dielectric strength with thickness suggests the presence of a strong gradient of molecular mobility along the distance from the metallic interfaces.The temperature dependence of the penetration depth of the interfacial interactions on the structural relaxation is further determined. The dynamic length scale of the perturbations into the chain conformations responsible for the deviation from bulk behavior is estimated based on the broadening effect of the α-peaks with decreasing film thickness.

2. EXPERIMENTAL SECTION

Materials and Sample Preparation. Poly(bisphenol A carbonate) (PBAC, Aldrich Chemical Co.) with a molecular weight of M_w = 22 000 g/mol and a polydispersity index of 1.23 is used in this study. The chemical structure is given in the inset of Figure 1a. The glass transition temperature T_g of the bulk material determined by DSC is 153.0 °C (426.2 K; heating rate 10 K/min; second heating run).

For the dielectric measurements the thin films were prepared between two thin aluminum electrodes where glass slides with size of 10 × 10 × 1 mm were used as substrate. The procedure to clean the substrates is described in detail in ref 37. In brief, the slides were first cleaned in an ultrasound alkaline bath at 333 K for 15 min followed by a second ultrasound bath with ultrahigh purified water (Millipore,

dx.doi.org/10.1021/ma202127p | Macromolecules 2012, 45, 1652−1662

resistivity >18 MΩ/cm). Then the glass plates were first rinsed in acetone and second in chloroform (both solvents Uvasol quality). After that, the substrates were dried in a nitrogen flow. An aluminum strip (width 2 mm, height ca. 60 nm) was deposited onto the glass substrate by thermal evaporation in an ultrahigh vacuum (10^{-5} mbar). After the evaporation of this first electrode the plates were again rinsed in acetone and chloroform. Subsequently, thin films with various thicknesses were obtained by spin-coating the filtered (minipore, 0.2 μm) solutions of PBAC in dichloromethane (5000 rpm, 50 s). The film thickness was varied by changing the concentration of the polymer solution. After spin-coating, all samples were annealed at 443 K ($T_{ann} = T_{g,Bulk} + 17$ K) in an oil-free vacuum for 24 h in order to remove the residual solvent and stress induced by the spin-coating procedure[56] and, meanwhile, to ensure the same well-defined thermal histories of all samples before the experiments. AFM topography images before and after the annealing procedure further show that down to 10 nm the film had a low roughness and no sign of dewetting was observed.

The preparation of the sample capacitor was finished by the evaporation of the counter electrode on the top of the polymer film in an ultrahigh vacuum (10^{-5} mbar). In general the evaporation of metals can damage the polymer surface as discussed in ref 21. To minimize the diffusion of metal atoms into the film and to avoid a damage of the polymer, a so-called flash evaporation (>30 nm/s) was applied. It is known that under these conditions a sharp and smooth metal/polymer interface is obtained.[57] It should be noted that a thin aluminum oxide layer (1−2 nm) might be formed at the bottom electrode.[58] This layer can influence the dielectric behavior, but equivalent circuit models can be applied to estimate its influence.

The film thickness d was determined by measuring the real part of the sample capacitance C' in a temperature and frequency region rarely affected by dielectric dispersions (T = 298 K, f = 1 kHz). It holds

$$d = \frac{\varepsilon_0 \varepsilon' A}{C'} \tag{1}$$

with ε_0 the permittivity of free space and A the electrode area (4 mm^2). ε' is the permittivity of the bulk sample estimated to be 3 at T = 298 K for 1 kHz. For a few samples this procedure was checked by the absolute thickness measurements by atomic force microscopy.

The corresponding bulk sample was obtained by casting a polymer/dichloromethane solution (15 wt %) on a polished glass substrate. To control the initial evaporation of the solvent from that thick film, the glass plate was placed in a closed chamber. To remove the residual solvent, the bulk sample was annealed under the same conditions as for the ultrathin films ($T_{ann} = T_{g,Bulk} + 17$ K in an oil-free vacuum (10^{-3} mbar) for 24 h. The sample thickness was 60 μm.

Methods. A high-resolution ALPHA analyzer (Novocontrol) is used to measure the complex dielectric function $\varepsilon^*(f) = \varepsilon'(f) - i\varepsilon''(f)$ (f = frequency, ε' and ε'' = real and imaginary part of the complex dielectric function, $i = (-1)^{1/2}$) in the frequency range from 10^{-1} to 10^7 Hz. The temperature was controlled by a Quatro Novocontrol cryosystem with a stability better than 0.1 K. For more details see ref 59. During the whole measurement the sample was kept in a pure nitrogen atmosphere.

To estimate the interfacial energy between aluminum oxide AlO_x and polycarbonate, contact angle measurements were carried out. The measurements were carried out using an automated contact angle system G2 (Krüss) employing the static sessile drop method. The probe liquids used were ethylene glycol, formamide, and water. Usually 8 drops with a volume of 3 μL were dropped onto the surface of the sample or the substrate. The reported contact angles were calculated from the average of at least 6 drops.

3. RESULTS AND DISCUSSION

As known in the literature, bulk polycarbonate shows at least two relaxation processes indicated by peaks in the dielectric loss ε'' (see Figure 1a). The β-relaxation (sometimes also called γ-relaxation) at low temperatures is assigned to localized fluctuations.[60] At temperatures higher than the β-process, the α-relaxation (dynamic glass transition) takes place. The paper is organized as follows. First, the dielectric properties of bulk polycarbonate are briefly discussed. Second, the thermal and dynamic glass transition of ultrathin films of supported PBAC films are discussed in detail by employing dielectric diletometry expansion and dielectric spectroscopy. Third, the influence of a nanometer confinement on the β-process of polycarbonate is commented.

Dielectric Relaxation of Bulk Polycarbonate. Recently, the β-relaxation of polycarbonate was investigated systematically by dielectric relaxation spectroscopy and neutron scattering.[61,62] It was found that the β-relaxation consists at least of two processes.[61] (In ref 61, a third relaxation process with a weak intensity is further discussed.) This is also found for the PBAC investigated here (see Figure 1b). The carbonyl group is the only polar structure in the repeat unit of PBAC and should be therefore involved in the β-relaxation. But there are longstanding discussions that the phenyl ring should be involved in that relaxation process.[63,64] A detailed comparison of the dielectric data with the results obtained from NMR and neutron scattering yields to the conclusion that the low-frequency part of the β-process is also related to the phenylene π-flips, and the 90° rotation of the phenylene rings became dominant in the high-frequency flank of the loss peak part.[61] It was further concluded that both processes are strongly coupled.

The model function introduced by Havriliak/Negami[65] (HN function) is used to analyze the dielectric measurements quantitatively. It reads

$$\varepsilon^*_{HN}(\omega) - \varepsilon_\infty = \frac{\Delta\varepsilon}{(1 + (i\omega/\omega_0)^\beta)^\gamma} \tag{2}$$

where ω_0 is a characteristic frequency related to the frequency of maximal loss f_p (relaxation rate). $\Delta\varepsilon$ denotes the dielectric strength. ε_∞ describes the value of the real part ε' for $\omega \gg \omega_0$. β and γ are fractional parameters ($0 < \beta \leq 1$ and $0 < \beta\gamma \leq 1$) characterizing the shape of the relaxation time spectra. From the fit of the HN function to the data the relaxation rate f_p and the dielectric strength are determined and further discussed. Conduction effects are treated in the usual way by adding a contribution $\varepsilon''_{cond} = \sigma_0/[\omega^s \varepsilon_0]$ to the dielectric loss where σ_0 is related to the specific dc conductivity of the sample. The parameter s ($0 < s \leq 1$) describes for s = 1 Ohmic and for $s < 1$ non-Ohmic effects in the conductivity. If two relaxation processes are observed in the experimental frequency window, a sum of two HN functions is fitted to the experimental data. For details see ref 66. An example for that procedure is given in Figure 1b, where two HN functions are fitted to the data of the β-relaxation of polycarbonate.

Figure 2 gives the temperature dependence of the relaxation rates for the α-relaxation for bulk polycarbonate. As is known for glassy dynamics, $f_{p,\alpha}(T)$ is curved versus $1/T$ which can be described by the Vogel−Fulcher−Tammann (VFT) equation[67]

$$\log f_p = \log f_\infty - \frac{A}{T - T_0} = \log f_\infty - \frac{\ln(10) D T_0}{T - T_0} \tag{3}$$

f_∞ and A are parameters where T_0 is called ideal glass transition or Vogel temperature which is found 30−70 K below the thermal glass transition temperature. D is the so-called fragility parameter or fragility strength and provides among others a

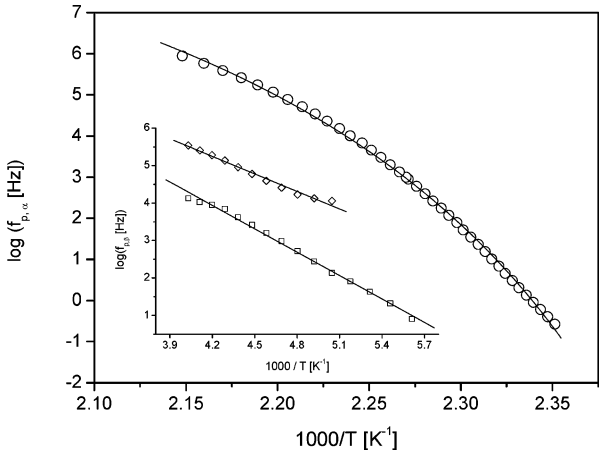

Figure 2. Relaxation rate $f_{p,\alpha}$ vs $1/T$ for the α-relaxation of bulk polycarbonate. The line is a fit of the VFT equation to the data. The inset gives $f_{p,\beta}$ vs $1/T$ for the both components of the β-relaxation of bulk PBAC: diamond, phenyl ring rotations; square, phenyl ring π-flips. The lines are fits of the Arrhenius equation to the corresponding data.

useful quantity to classify glass-forming systems.[68,69] Polymers are called "fragile" if their $f_p(T)$ dependence deviates strongly from an Arrhenius-type behavior and "strong" if $f_p(T)$ is close to the latter.

For the two components of the β-relaxation the temperature dependence of the relaxation rate obeys the Arrhenius equation (see inset of Figure 2)

$$\log f_p = \log f_\infty - \frac{\ln(10) E_A}{k_B T} \quad (4)$$

where E_A is the activation energy and k_B is the Boltzmann constant. The following activation parameters are estimated: phenyl ring rotations, E_A = 29.9 kJ/mol; $\log(f_\infty\ [\mathrm{Hz}])$ = 11.8; phenyl ring π-flips, E_A= 39.8 kJ/mol; $\log(f_\infty\ [\mathrm{Hz}])$ = 12.7. These values are in agreement with data from the literature.[61]

Dielectric Expansion Dilatometry. Dielectric expansion dilatometry relies on the analysis of the temperature dependence of the dielectric permittivity $\varepsilon'(T)$ for thin films under the assumption that no dielectric active processes take place in the selected frequency and temperature range. Its theoretical basis is considered in detail in ref 70. The real part of the permittivity can be expressed by $\varepsilon'(f_e,T) = \varepsilon_\infty(T) + \Delta\varepsilon(f_e,T)$ where $\Delta\varepsilon$ is related to a dielectric dispersion due to molecular fluctuations, ε_∞ is the real part of the permittivity in the high frequency limit, and f_e is the detection frequency. For a parallel plate capacitor in the described thin film geometry the temperature dependence of the geometrical capacitance $C_0(T) = \varepsilon_0[A/\mathrm{d}(T)] \sim \varepsilon_0(A/d_R)(1 - \alpha(T)\Delta T)$, where ΔT is a temperature change with regard to a reference temperature T_R ($T = T_R + \Delta T$), $d(T)$ is the thickness of the film in dependence of the temperature ($d_R = d(T_R)$), and A is the electrode area.[70] $\alpha(T)$ is the thermal expansion coefficient normal to the film surface. If the detection frequency f_e is set to such a value that no relaxation process is present ($\Delta\varepsilon \approx 0$), the temperature dependence of ε' is given by $\varepsilon'(T) = \varepsilon_\infty(T) \sim \varepsilon_\infty(T_R)(1 - \alpha(T)\Delta T)$. For polymers with a relatively weak dipole moment like polycarbonate this approach can be used to estimate a thermal glass transition temperature T_g from the change in the temperature dependence of ε' at sufficiently high frequencies, i.e., outside the appearance of the α-relaxation.

Figure 3 gives the temperature dependence of ε' normalized to the value at T = 380 K to get rid of temperature change due

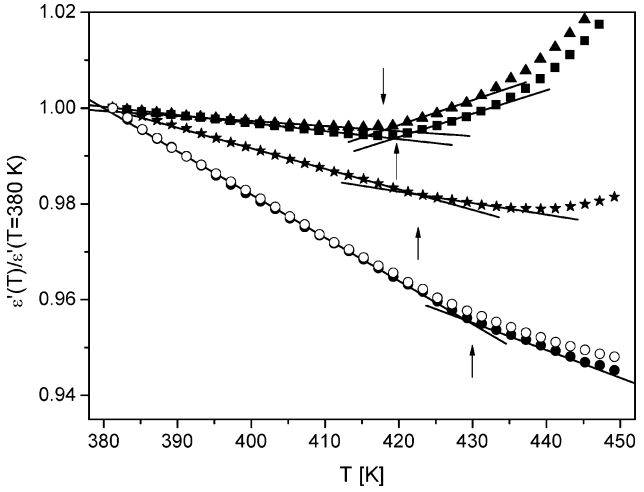

Figure 3. Temperature dependence of the dielectric permittivity ε' normalized with respect to its values at T = 380 K for a frequency of 10^5 Hz for different film thicknesses d: filled triangles, bulk; filled squares, 198 nm; filled stars, 47 nm; filled circles, 13 nm. The solid lines are linear fits of the data. The arrows indicate the values of T_g. The open circles are data for the 13 nm film measured for a frequency of 10^4 Hz. It is shown that the effect of the dielectric dispersion is quite weak above 10^4 Hz.

to the β-relaxation for several film thicknesses. For all values of the film thickness the real part of the complex permittivity decreases with increasing temperature up to a given temperature where the temperature dependence of ε' changes. This change in the temperature dependence of ε' is due to the change of the expansion coefficient at the thermal glass transition as discussed above. The initial deviation of the dielectric permittivity from a linear temperature is used to extract the thermal glass transition temperature (see Figure 3), which is plotted versus the thickness of the layer in Figure 4. The increase of ε' at higher temperatures is due to the contribution of the α-relaxation.

Figure 4 shows that down to a film thickness of ca. 20 nm T_g is more or less independent of the film thickness or increases slightly. For thicknesses lower than 20 nm an increase of T_g with decreasing d is observed. This behavior is quite similar to that found for polysulfone[37] and points to a strong interaction of polycarbonate with the aluminum substrates which leads to the formation of an adsorbed boundary layer with a reduced mobility.

Dielectric Spectroscopy on Thin Films. Different from the dielectric spectroscopy on bulk samples discussed above for the thin film geometry one has to consider that the resistance R of the Al electrodes cannot be neglected. This resistance leads to an artificial loss peak (electrode peak) on the high-frequency side of the spectra with a time constant $\tau_{Res} = RC'$ (C' = sample capacity). The electrode peak shifts to lower frequencies because with decreasing film thickness the sample capacity C' increases. The frequency dependence of the electrode peak obeys a Debye function. For optimized sample geometries the maximum position of this electrode peak $f_{Res} \sim 1/\tau_{Res}$ can be shifted outside the experimental accessible frequency window. Therefore, the Debye function can be approximated by its low-frequency tail, and the complete function reads as

dx.doi.org/10.1021/ma202127p | Macromolecules 2012, 45, 1652–1662

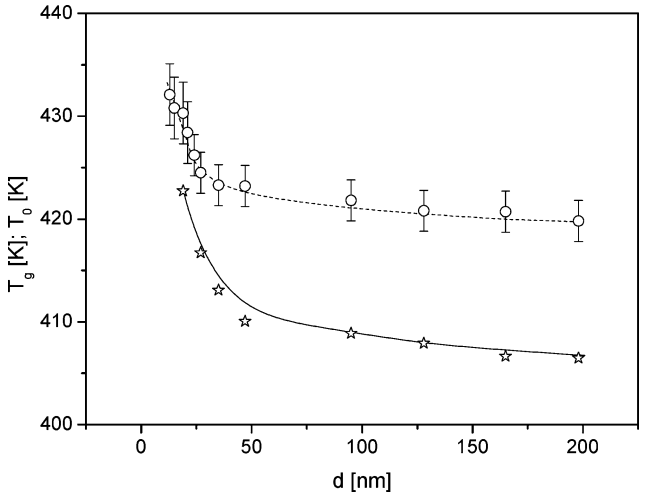

Figure 4. Circles: glass transition temperature T_g as measured by dielectric expansion dilatometry versus film thickness. The dotted line is a guide for the eyes. Stars: Vogel temperature T_0 vs film thickness. The solid line is a guide for the eyes.

$$\varepsilon^*_{\mathrm{Fit}} = \varepsilon^*_{\mathrm{HN}}(\omega) + i\frac{\sigma}{\omega^s \varepsilon_0} + iB^*\omega \tag{5}$$

where B is a fitting parameter mainly related to τ_{Res}. Figure 5 gives an example for the analysis of the dielectric spectra of a thin polycarbonate film with a thickness of 47 nm.

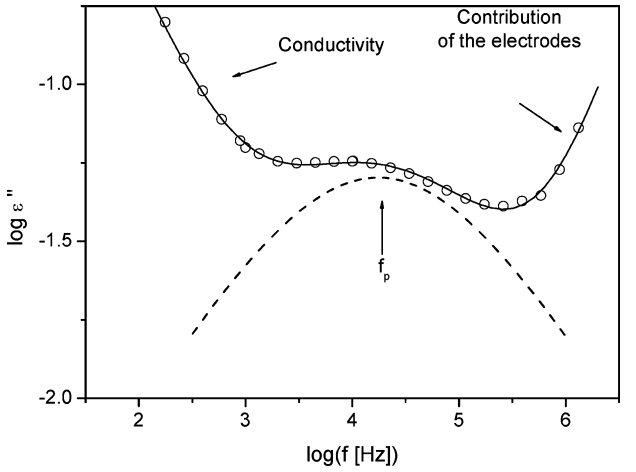

Figure 5. Dielectric loss versus frequency of a polycarbonate film with a thickness of 47 nm at T = 449 K. The solid line is a fit of eq 5 to the data. The dashed line gives the contribution of the α-relaxation.

The thin polycarbonate films show a relatively strong conductivity contribution. Therefore, the analysis of the dielectric spectra is restricted to higher frequencies and to a narrower temperature range compared to the bulk sample. The reason for the enhanced conductivity contribution might be an arrangement of the phenyl rings parallel to the electrodes.

In Figure 6, the relaxation rate $f_{p,\alpha}$ is plotted versus $1/T$ for different film thicknesses. Besides for the lowest layer thickness all other data are collapsing into one chart. This is in agreement with the results obtained by dielectric expansion dilatometry (see Figure 4). For the lowest film thickness the whole curve is shifted to higher temperatures. To analyze the temperature dependence of the relaxation rate in more detail, a derivative

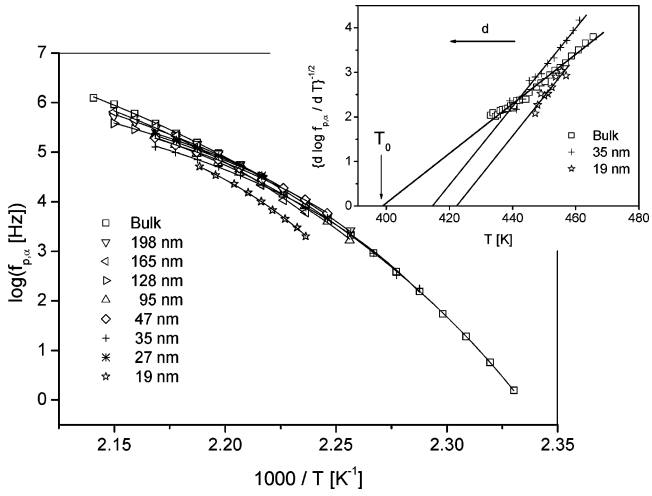

Figure 6. Relaxation rate $f_{p,\alpha}$ versus $1/T$ for the α-relaxation of polycarbonate films for the labeled film thicknesses. Lines are fits of the VFT equation to the corresponding data as described in the text. The inset gives $[(\mathrm{d}\log f_{P,\alpha})/\mathrm{d}T]^{-1/2}$ versus temperatures for labeled thicknesses. Lines are linear regressions to the data.

method is used.[71] With this method the temperature dependence of $f_{p,\alpha}$ can be analyzed in detail irrespective of the prefactor. For a temperature dependence according to the VFT equation

$$\left[\frac{\mathrm{d}\log f_p}{\mathrm{d}T}\right]^{-1/2} = A^{-1/2}(T - T_0) \tag{6}$$

is obtained. This means in a plot $[\mathrm{d}\log f_p/\mathrm{d}T]^{-1/2}$ versus T a VFT behavior shows up as a straight line (see inset of Figure 6). Besides the linearization of the data, the number of free fit parameters is reduced which increases the significance of the estimated parameters. Because all experimental data given in the inset of Figure 6 can be well described by straight lines, it is concluded that for all thicknesses the relaxation rates follow the VFT temperature dependence.

The following procedure was applied to estimate the parameters of the VFT equation and the fragility strength D for a quantitative comparison. T_0 and A were taken from the derivative technique by linear regression. The prefactors were obtained by a fit of the VFT equation to the relaxation rates keeping T_0 and A fixed. The parameters are collected in Table

Table 1. Estimated VFT Parameters and Glass Transition Temperatures T_g

thickness (nm)	log(f_∞ [Hz])	A (K)	T_0 (K)	T_g (K)	$D = A/T_0 \ln(10)$
bulk	13.22	573.4	385.0	418.5	0.646
198	9.82	242.4	406.5	419.8	0.259
165	9.68	225.3	406.6	420.7	0.240
128	8.91	190.0	407.9	420.8	0.202
95	8.95	181.9	408.8	421.8	0.193
47	8.60	169.8	410.0	423.2	0.179
35	8.24	163.8	413.1	423.3	0.172
27	8.34	131.8	416.7	424.5	0.137
19	8.20	119.4	422.7	430.3	0.122

1. As discussed above for the thin films the investigated temperature is narrower than for the bulk sample. This might

dx.doi.org/10.1021/ma202127p | Macromolecules 2012, 45, 1652–1662

complicate a direct comparison of the data point for the bulk with data for the thin films. But for the thin films a similar temperature range is analyzed where the thickness of the sample varies by more than 1 order of magnitude. Therefore, the data for the thin films can be compared directly.

The Vogel temperature T_0 shows a similar dependence on the film thickness as the glass transition temperature T_g estimated by dielectric expansion dilatometry which indicates that both data sets analyzed independently from each other are consistent. Down to a film thickness of ca. 20 nm, T_0 is more or less independent of the film thickness or increases slightly. For thicknesses lower than 20 nm an increase of T_0 with decreasing d is observed (see Figure 4). For thicknesses lower than 20 nm a strong increase of T_0 with decreasing d is observed as also found for other systems.[12,42,44] This will be discussed in detail later.

The fragility strength D is calculated from the estimated VFT parameters and plotted versus $1/d$ in Figure 7. It is shown that

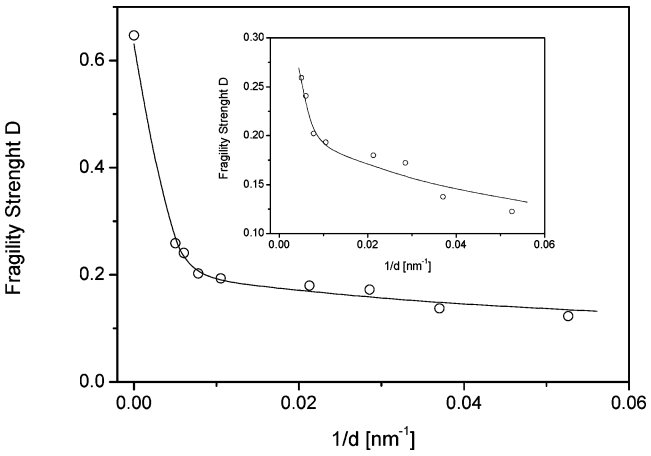

Figure 7. Fragility strength D versus inverse film thickness. The line is a guide for the eyes. The inset compares the data only for the thin films. The line is a guide for the eyes.

the fragility strength decreases with deceasing film thickness but seems to reach a plateau value for low values of d.

The dielectric strength $\Delta\varepsilon$ is obtained in addition to the relaxation rate from the fit of the HN function to the data. The Debye theory of dielectric relaxation generalized by Kirkwood and Fröhlich[72] expresses this quantity as a function of the temperature T

$$\Delta\varepsilon = \frac{1}{3\varepsilon_0} g \frac{\mu^2}{k_B T} \frac{N}{V} \tag{7}$$

The Onsager factor is omitted for sake of simplicity, ε_0 is the permittivity of the vacuum, N/V is the number density of dipoles involved in the relaxation process, and μ is the mean dipole moment of the process under consideration. g denotes the so-called Kirkwood–Fröhlich factor, which describes static correlation between the dipoles. For several layer thicknesses $\Delta\varepsilon$ is plotted versus temperature in Figure 8.

In Figure 9, $\Delta\varepsilon$ is plotted as a function of the inverse layer thickness (equivalent to the surface/volume ratio in the thin film geometry) at T = 450 K. As a general feature of the α-relaxation under confinement, the dielectric strength decreases in the thinnest films. This trend was explained in terms of chain adsorption,[73] as the dipole moment does not depend on the

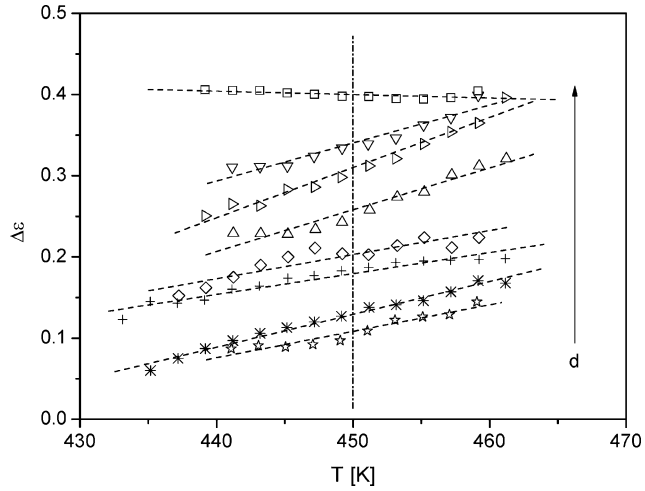

Figure 8. $\Delta\varepsilon$ versus temperature for different film thicknesses: squares, bulk; down side triangles, 198 nm; right side triangles, 128 nm; up sided triangles, 95 nm; diamonds, 47 nm; crosses, 35 nm; stars, 27 nm; full stars, 19 nm. The dashed line is a guide for the eyes. The dotted-dashed line indicates for the temperature comparison.

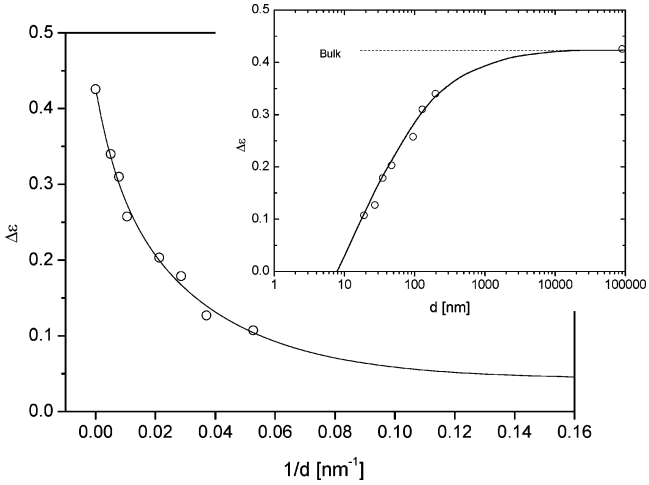

Figure 9. $\Delta\varepsilon$ vs inverse film thickness for T = 450 K. The inset gives $\Delta\varepsilon$ vs d. Lines are guides for the eyes.

film thickness. The decrease of $\Delta\varepsilon$ is due to a strong reduction of the number density of fluctuating dipoles in proximity of the interface, a hypothesis also proven by measurements of the local dielectric strength in multilayer experiments.[36] In the specific case of the polymer–metal system investigated, this idea is further confirmed by the high interfacial energy between polycarbonate and AlO_x (see below), inhibiting the motion of the segments close to the electrodes on the time and the length scale of the glass transition.

The observed pronounced nonlinear reduction of the dielectric strength upon increase of the surface-to-volume ratio suggests the presence of a strong gradient of molecular mobility along the distance from the metallic interfaces. To understand such a profile, the impact of the thickness on the temperature dependence of the dielectric strength was also analyzed (see Figure 8).

Contrary to the prediction of eq 7 valid for the structural relaxation of bulk systems, in thin films $\Delta\varepsilon$ increases with increasing temperature, a behavior was previously observed also in other polymer film of comparable thickness.[42,43] This

dx.doi.org/10.1021/ma202127p | Macromolecules 2012, 45, 1652–1662

anomalous trend is the entanglement of two different phenomena, i.e., the reduction of the number density of fluctuating dipoles in proximity of a bounding interface coupled to the impact of thermal energy on the defreezing of segmental motion.[74,75] Increasing the temperature induces a gradual release of the constraints affecting the segmental dynamics, which yields to the anomalous increase of dielectric strength upon heating.

We quantitatively determined the temperature dependence of the penetration depth of the interfacial interactions on the structural relaxation, applying an analysis recently proposed by Rotella et al.[73] The profiles of mobility, based on the density number of dipoles participating to the structural relaxation, were built up mimicking the usual dependence of density in proximity of an interface, via a function symmetric with respect to the center of the film

$$\Delta\varepsilon(x) = \Delta\varepsilon^{BULK}\left[\tanh^2\left(3\frac{x}{\phi} + \rho\right) + \tanh^2\left(3\frac{d-x}{\phi} + \rho\right) - \tanh^2\left(3\frac{d}{\phi} + \rho\right)\right] \quad (8)$$

where x is the distance from the interface, φ the length scale of the reduction of $\Delta\varepsilon$, and ρ a parameter taking account the residual polarization at the interface, as $\tanh^2(\rho) = \Delta\varepsilon(0)/\Delta\varepsilon_{bulk}$.

To obtain the best fitting parameter for each data set (i.e., $\Delta\varepsilon(d)$ in isothermal condition), the experimental data were compared to values calculated via eq 8. The procedure required the calculation of the total dielectric response of a film of thickness d, via a layer resolved approach, whose validity is supported by previous simulation work on the dielectric relaxation at the nanoscale.[76]

The film is divided into d sublayers, i.e., with a resolution of 1 nm; at each sublayer, we attributed a dielectric function reproduced by the HN equation (see eq 2). The position and the shape of the peak of each sublayer are kept constant where the dielectric strength is varied, following a profile given by discretization of eq 8 in steps of 1 nm. Considering the orientation of the electric field in our experiments (perpendicular to the polymer/metal interface), the total dielectric response was obtained summing up the contributions of all the sublayers as for capacitors in series, $C_{TOT}^{-1}(f,T) = \sum_j C_j^{-1}(f,T)$, where $C_j(f,T)$ is the capacitance of the jth sublayer. In our computation, the value of $\Delta\varepsilon_{TOT}$ was obtained directly from the real part of the dielectric function following its definition[77] as the difference between ε_S, the frequency independent value reached by the real part of the dielectric function for $\omega \ll \omega_0$, and ε_∞. We considered a frequency range broad enough to take into account the broadening of the structural peak, i.e., a larger separation between the frequency regions corresponding to ε_S and ε_∞, and the shift in the peak maximum upon confinement. Moreover, to limit the number of free parameters, we kept the shape parameters and the position of the peak in the sublayers constant. This is justified by our previous work[36,49] where we verified that in ultrathin films of amorphous polymers the dielectric strength depends on the interaction with the substrate and on the annealing conditions used. (In the samples analyzed in our work γ^{TOTAL} was constant, and samples were prepared under the same annealing conditions.) This procedure is repeated for a matrix of couples (φ^i, ρ^i) centered around physically reasonable starting parameters and found the best fitting values for the experimental values in Figure 10, upon minimization of the

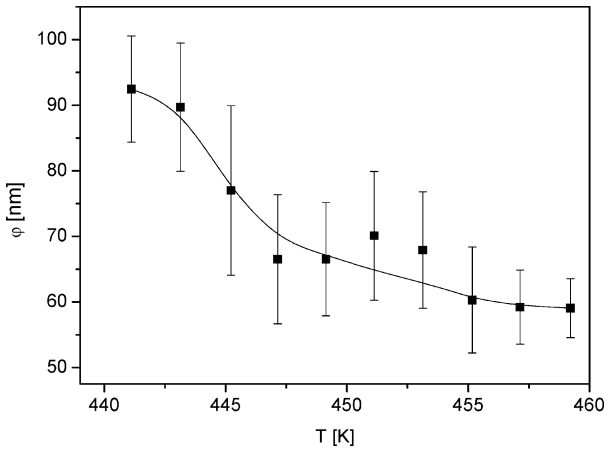

Figure 10. Temperature dependence of the penetration depth φ.

squared deviations: Err = $(1/n_{exp})\sum_{i=1}^{n_{exp}}[(\Delta\varepsilon_i^{th} - \Delta\varepsilon_i^{exp})/\Delta\varepsilon_i^{exp}]^2$, where n_{exp} is the number of the experimental data points, i.e., the number of thicknesses measured at each temperature, and $\Delta\varepsilon^{th}$ and $\Delta\varepsilon^{exp}$ are respectively the values of the dielectric strength obtained via the model and experimentally. The obtained values are plotted in Figure 10. At 443 K, φ reaches 90 nm, a value which is comparable to, although slightly larger than, that of PET in the same dynamic range. Compared to more flexible polymers, where φ does not exceed 40 nm, the relatively longer length scale reflects the rigidity of the chains of PBAC. The less flexibility combined to the previously mentioned arrangement of the phenyl rings parallel to the electrodes induces a residual polarization at the interface on the order of 20% of the bulk value, i.e., $\rho \sim 0.5$, responsible for the nonzero value of $\Delta\varepsilon$ in the thinnest films. The temperature dependence of the penetration depth of the interfacial interactions increases upon cooling with an activation energy 10-fold smaller than the structural relaxation. Such a trend is in line with what is observed in ultrathin films of polystyrene labeled with polar moieties[73] and what is predicted by molecular dynamics simulations.[78]

The presence of a profile of mobility affecting the dynamics of the film[79,80] is reflected also in the thickness dependence of the width of the α-peak, which broadens upon reduction of the thickness (see Figure 11). This broadening arises from the heterogeneity in the molecular dynamics, related to the introduction of slower modes in the distribution of relaxation times. At the polymer/metal interface, in fact, the mobility of chains is hindered down to the segmental motion, due to less available space[81] and the favorable interactions with the aluminum surface. The perturbations into the chain conformations responsible for such deviation from bulk dynamics vanish after a dynamic length scale λ. It is possible to estimate λ by an analysis of the thickness dependence of the broadening of the α-peak in capped films, based on simple considerations on samples with symmetric interfaces.[82] In thick films, $d \gg \lambda$, the volume fraction of segments relaxing like in bulk is predominant and the width is thickness independent. Upon thickness reduction, the weight of interfacial layers on the total

dx.doi.org/10.1021/ma202127p | Macromolecules 2012, 45, 1652–1662

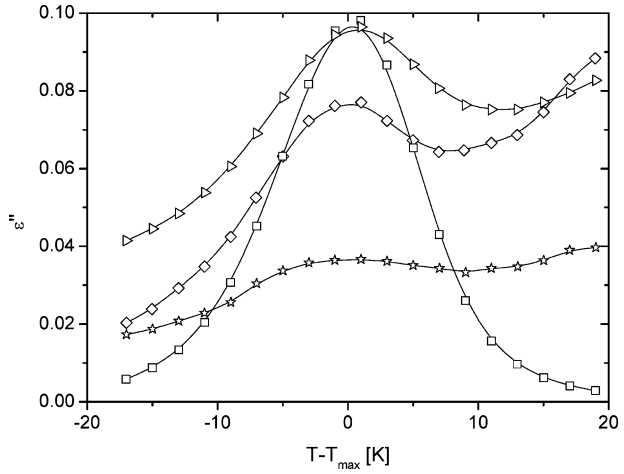

Figure 11. Dielectric loss versus normalized temperature at 1 kHz for different film thicknesses: squares, bulk; right side triangles, 95 nm; diamonds, 47 nm; full stars, 19 nm. The lines are guides for the eyes.

dielectric signal increases, and because of the different time scale of the segmental relaxation at the interface,[36] the α-peak broadens in the frequency domain. Such a confinement induced broadening reaches a maximum in proximity of 2λ, where the bulk component disappears. Further reduction of the thickness corresponds to a cutoff of those modes relaxing like in bulk, which leads to a reduction of the broadening. For PBAC, in the thickness range where it was possible to determine univocally the shape of the structural peak, i.e., down to 19 nm, only a broadening of the α-peak is observed. Consequently, we can estimate that, at each interface, the interaction with the metallic substrate affects the dynamics for a length scale $\lambda \leq 9$ nm. This critical length is in line with the trends in the thickness dependence of T_g and T_0 (see Figure 4) where no confinement effect is observed for films where the separation between the two metallic layers exceeds 20 nm.

Such a dynamic length scale is much smaller than that determined via the thickness dependence of the dielectric strength, a trend in line with the behavior of almost all polymer systems investigated at the nanoscale.[73] The origin of this apparent discrepancy stays in the different averaging rules affecting the intensity ($\Delta\varepsilon$) and the shape (peak maximum, broadness, asymmetry) of a relaxation peak,[75] which permit to observe a perturbation in the dynamics only at higher surface/volume ratios (thinner films) compared to those of interest to static properties like the dielectric strength.

To confirm the strong interaction between aluminum oxide AlO_x and polycarbonate, contact angle measurements were carried out. The angle values are given in Table 2. The contact

Table 2. Contact Angle Values of the Test Liquids with Polycarbonate[a]

	ethylene glycol	formamide	water
poly(bisphenol A carbonate)	67.6 ± 0.47	71.8 ± 0.7	93.0 ± 0.35

[a]The error bars results from the average of the measurements on 8 drops.

angle values were used as input to calculate the interfacial energy γ_{SP} in the frame of the Fowkes–van Oss–Chaudry–Good (FOCG) model.[83] The surface tension is given by $\gamma^{Total} = \gamma^{LW} + \gamma^{P} = \gamma^{LW} + 2(\gamma^{+}\gamma^{-})^{1/2}$, where γ^{LW} is the dispersive and γ^{P} the polar component. The polar component is further expressed by the electron acceptor γ^{+} and the electron donor component γ^{-}.[83,84] γ^{LW},γ^{+}, and γ^{-} were estimated by solving the system of the corresponding Young and Dupré[83] equations (system of three equations)

$$(1 + \cos\theta_i)\gamma^{PC} = 2[(\gamma_{PC}^{LW}\gamma_{L,i}^{LW})^{1/2} + (\gamma_{PC}^{+}\gamma_{L,i}^{-})^{1/2} + (\gamma_{PC}^{-}\gamma_{L,i}^{+})^{1/2}] \quad (9)$$

using the contact angles θ_i measured for each test liquid i. PC symbolizes polycarbonate and L the test liquids where the corresponding values for the test liquids were taken from ref 84 (see Table 3). The values obtained for both aluminum and

Table 3. Total Surface Energy γ^{Total} and Its Dispersive γ^{LW} and Polar Component γ^{P} for the Test Liquids According to the Data Given in Ref 84

	ethylene glycol	formamide	water
γ^{total} [mJ/m^2]	48.0	58	72.8
γ^{LW} [mJ/m^2]	29	39	26
γ^{+} [mJ/m^2]	2.60	3.1	34.2
γ^{-} [mJ/m^2]	34.8	29.1	19

Table 4. Total Surface Energy γ^{Total} and Its Dispersive γ^{LW} and Polar Component γ^{P} for Polycarbonate and Aluminum Oxide[a]

	γ^{total} [mJ/m^2]	γ^{LW} [mJ/m^2]	γ^{+} [mJ/m^2]	γ^{-} [mJ/m^2]
poly(bisphenol A carbonate)	33.21	32.95	0.03	0.56
aluminum	30.4	26.5	0.5	7.7

[a]The data for aluminium were taken from ref 42.

polycarbonate are displayed in Table 4. The combining rule of Good–Girifalco–Fowkes[85] was applied to estimate γ_{SP} between PBAC and AlO_x

$$\gamma_{SP} = (\sqrt{\gamma_S^{LW}} - \sqrt{\gamma_P^{LW}})^2 + 2[(\gamma_S^{+}\gamma_S^{-})^{1/2} + (\gamma_P^{+}\gamma_P^{-})^{1/2} - (\gamma_S^{+}\gamma_P^{-})^{1/2} - (\gamma_S^{-}\gamma_P^{+})^{1/2}] \quad (10)$$

S and P refer to the substrate and the polymer. The data for aluminum are taken from ref 42. The dispersive part of the AlO_x/PBAC is calculated to be 0.35 mJ/m^2, and the polar one is 2.16 mJ/m^2, leading to a total energy of 2.51 mJ/m^2. This value is higher than the critical value discussed in ref 47 ($\gamma^{*}_{sp} \approx$ 2 mJ/m^2 for different couples of substrates and polymers), corresponding to an increase of T_g as observed in the dielectric experiments. The real interfacial energy could be however higher than the calculated γ_{SP} due to the formation of chemical bonds or specific interaction between Al and PBAC. The interfacial chemical interaction between spin-coated polycarbonate and thermally evaporated aluminum has been studied by X-ray photoelectron spectroscopy in detail.[86] C=O and C–O entities of polycarbonate react with Al atoms to form an Al–O–C like complex. Al–C bonding also forms due to the interaction between phenyl ring and Al atoms. Aluminum oxide (O–Al) and aluminum hydroxides (HO–A1) can be detected

dx.doi.org/10.1021/ma202127p | Macromolecules 2012, 45, 1652–1662

at the Al/PBAC interface. The formation of these chemical bonds contributes to the attractive interfacial interaction between PBAC and Al layers.

To discuss the dielectric data in more detail, the loss part is plotted at a frequency of 1 kHz versus temperature for the bulk sample and for films with different thicknesses (Figure 12).

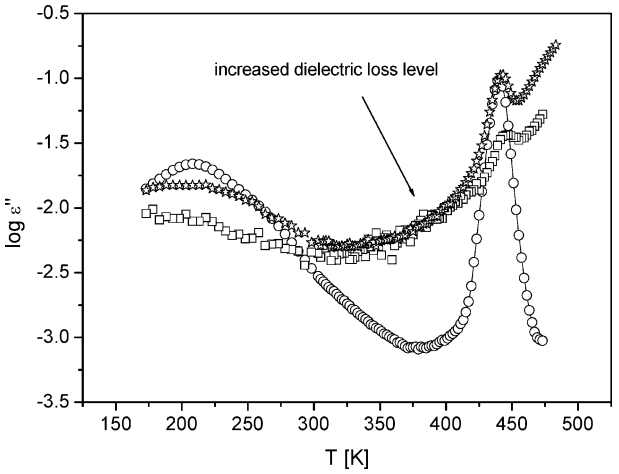

Figure 12. Dielectric loss versus temperature at a frequency of 1 kHz: circles, bulk polycarbonate; squares, 128 nm; stars, 19 nm.

Compared to the bulk sample for the thin film, the dielectric loss is significantly increased for temperatures below the α-relaxation.[87] By convention, a glass transition temperature can be defined by the maximum temperature of the α-relaxation which corresponds only to one point of the whole spectra. Any finite value of the dielectric loss corresponds to certain molecular fluctuations or motions (see ref 88). It might be that different aspects of the molecular mobility which leads to different definitions of the glass transition temperature and therefore to different thickness dependencies.

Thickness Dependence of the β-Relaxation. In addition to the facts discussed above, Figure 12 reveals also that the intensity of the β-relaxation peak decreases with the decreasing film thickness and cannot be observed for thinnest film. As discussed above, the β-relaxation is assigned to different motional modes of the phenyl ring. The observed decrease in the intensity of the β-process means that the phenyl rings are immobilized by the polymer−substrate interaction. Likely is a planar arrangement of it to the surface. A reduction of the localized fluctuation in ultrathin polycarbonate films was also observed by neutron scattering.[10] Moreover, such a depression of the β-relaxation strength is in good agreement with previous dielectric studies of PMMA.[89]

4. CONCLUSION

Ultrathin films of poly(bisphenol A carbonate) capped between two aluminum layers were studied by dielectric expansion dilatometry and dielectric spectroscopy. The thermal glass transition temperature is more or less independent of the film thickness down to 20 nm. An increase of T_g is observed when the film thickness is lower than 20 nm. This is in agreement with the thickness dependence of the Vogel temperature. It is further found that the fragility decreases with decreasing film thickness until a plateau value is reached.

To explore the interaction of polycarbonate with aluminum surface, the dielectric relaxation strength was estimated from the measurements. It is proportional to the dipole density taking part in the α-relaxation process. A pronounced nonlinear reduction of the dielectric strength with decreasing film thickness was observed, which is attributed to the formation of a reduced mobility layer at the interface. Polycarbonate chains in the proximity of the interface have adsorption to the aluminum surface due to the strong interfacial interaction. The interfacial energy between polycarbonate and aluminum layers is quantitatively determined by contact angle measurements and related calculations. With further analysis based on the impact of the thickness on the temperature dependence of the dielectric strength, the temperature dependence of the penetration depth of the interfacial interactions on the structural relaxation is determined. The broadening of the α-peak with decreasing thickness is due to the heterogeneity in the mobility induced by the interaction of the segments with the surfaces. A dynamic length scale of the surface perturbations of the chain conformations is estimated to be smaller than 9 nm. This is in agreement with the thickness dependence of the glass transition and the Vogel temperature.

AUTHOR INFORMATION

Corresponding Author

*Tel: +49 30/8104-3384; Fax: +49 30/8104-1637; e-mail: Andreas.Schoenhals@bam.de.

Notes

The authors declare no competing financial interest.

ACKNOWLEDGMENTS

The authors gratefully acknowledge the assistance of D. Neubert for his experimental help. The financial support from the German Science Foundation (Deutsche Forschungsgemeinschaft, SCHO-470/20-1) is highly acknowledged.

REFERENCES

(1) Keddie, J. L.; Jones, R. A. L.; Cory, R. A. *Faraday Discuss.* **1994**, *98*, 219−230.
(2) Alcoutlabi, M.; McKenna, G. B. *J. Phys.: Condens. Matter* **2005**, *17*, R461−R524.
(3) Fakhraai, Z.; Forrest, J. A. *Phys. Rev. Lett.* **2005**, *95*, 025701.
(4) O'Connell, P. A.; McKenna, G. B. *Science* **2005**, *307*, 1760−1763.
(5) Napolitano, S.; Wübbenhorst, M. *Macromolecules* **2006**, *39*, 5967−5970.
(6) Zheng, X.; Rafailovich, M. H.; Sokolov, J.; Strzhemechny, Y.; Schwarz, S. A.; Sauer, B. B.; Rubinstein, M. *Phys. Rev. Lett.* **1997**, *79*, 241−244.
(7) Wallace, W. E.; van Zanten, J. H.; Wu, W. L. *Phys. Rev. E* **1995**, *52*, R3329−R3332.
(8) Reiter, G. *Macromolecules* **1994**, *27* (11), 3046−3052.
(9) Weber, R.; Zimmermann, K. M.; Tolan, M.; Stettner, J.; Press, W.; Seeck, O. H.; Erichsen, J.; Zaporojtchenko, V.; Strunskus, T.; Faupel, F. *Phys. Rev. E* **2001**, *64*, 061508.
(10) Soles, C. L.; Douglas, J. F.; Wu, W. l.; Dimeo, R. M. *Phys. Rev. Lett.* **2002**, *88*, 037401.
(11) Soles, C. L.; Douglas, J. F.; Wu, W. l.; Dimeo, R. M. *Macromolecules* **2003**, *36*, 373−379.
(12) Forrest, J. A.; Dalnoki-Veress, K.; Stevens, J. R.; Dutcher, J. R. *Phys. Rev. Lett.* **1996**, *77*, 2002.
(13) Cheng, W.; Sainidou, R.; Burgardt, P.; Stefanou, N.; Kiyanova, A.; Efremov, M.; Fytas, G.; Nealey, P. F. *Macromolecules* **2007**, *40*, 7283−7290.
(14) Efremov, M. Y.; Olson, E. A.; Zhang, M.; Zhang, Z.; Allen, L. H. *Phys. Rev. Lett.* **2003**, *91*, 085703.
(15) Lupascu, V.; Huth, H.; Schick, C.; Wübbenhorst, M. *Thermochim. Acta* **2005**, *432*, 222−228.

(16) Huth, H.; Minakov, A. A.; Schick, C. *J. Polym. Sci., Part B: Polym. Phys.* **2006**, *44*, 2996−3005.
(17) Tress, M.; Erber, M.; Mapesa, E. U.; Huth, H.; Müller, J.; Serghei, A.; Schick, C.; Eichhorn, K.-J.; Voit, B.; Kremer, F. *Macromolecules* **2010**, *43*, 9937−9944.
(18) Zhou, D.; Huth, H.; Gao, Y.; Xue, G.; Schick, C. *Macromolecules* **2008**, *41*, 7662−7666.
(19) Keddie, J. L.; Jones, R. A. L.; Cory, R. A. *Europhys. Lett.* **1994**, *27*, 59.
(20) Dalnoki-Veress, K.; Forrest, J. A.; Murray, C.; Gigault, C.; Dutcher, J. R. *Phys. Rev. E* **2001**, *63*, 031801.
(21) Sharp, J. S.; Forrest, J. A. *Phys. Rev. Lett.* **2003**, *91*, 235701.
(22) Lu, H.; Chen, W.; Russell, T. P. *Macromolecules* **2009**, *42*, 9111−9117.
(23) Erber, M.; Georgi, U.; Müller, J.; Eichhorn, K. J.; Voit, B. *Eur. Polym. J.* **2010**, *46*, 2240−2246.
(24) Clough, A.; Peng, D.; Yang, Z.; Tsui, O. K. C. *Macromolecules* **2011**, *44*, 1649−1653.
(25) Ellison, C. J.; Torkelson, J. M. *Nature Mater.* **2003**, *2*, 695−700.
(26) Mundra, M. K.; Ellison, C. J.; Rittigstein, P.; Torkelson, J. M. *Eur. Phys. J.: Spec. Top.* **2007**, *141*, 143−151.
(27) Priestley, R. D.; Broadbelt, L. J.; Torkelson, J. M.; Fukao, K. *Phys. Rev. E* **2007**, *75*, 061806.
(28) Kim, S.; Roth, C. B.; Torkelson, J. M. *J. Polym. Sci., Part B: Polym. Phys.* **2008**, *46*, 2754−2764.
(29) Ge, S.; Pu, Y.; Zhang, W.; Rafailovich, M.; Sokolov, J.; Buenviaje, C.; Buckmaster, R.; Overney, R. M. *Phys. Rev. Lett.* **2000**, *85*, 2340.
(30) Dinelli, F.; Ricci, A.; Sgrilli, T.; Baschieri, P.; Pingue, P.; Puttaswamy, M.; Kingshott, P. *Macromolecules* **2011**, *44*, 987−992.
(31) Xie, L.; DeMaggio, G. B.; Frieze, W. E.; DeVries, J.; Gidley, D. W.; Hristov, H. A.; Yee, A. F. *Phys. Rev. Lett.* **1995**, *74*, 4947.
(32) DeMaggio, G. B.; Frieze, W. E.; Gidley, D. W.; Zhu, M.; Hristov, H. A.; Yee, A. F. *Phys. Rev. Lett.* **1997**, *78*, 1524.
(33) Fukao, K.; Miyamoto, Y. *Phys. Rev. E* **2000**, *61*, 1743.
(34) Lupascu, V.; Picken, S. J.; Wübbenhorst, M. *J. Non-Cryst. Solids* **2006**, *352*, 5594−5600.
(35) Serghei, A.; Huth, H.; Schick, C.; Kremer, F. *Macromolecules* **2008**, *41*, 3636−3639.
(36) Rotella, C.; Napolitano, S.; Cremer, L. D.; Koeckelberghs, G.; Wübbenhorst, M. *Macromolecules* **2010**, *43*, 8686−8691.
(37) Labahn, D.; Mix, R.; Schönhals, A. *Phys. Rev. E* **2009**, *79*, 011801.
(38) Serghei, A.; Huth, H.; Schellenberger, M.; Schick, C.; Kremer, F. *Phys. Rev. E* **2005**, *71*, 061801.
(39) Huth, H.; Minakov, A. A.; Serghei, A.; Kremer, F.; Schick, C. *Eur. Phys. J.: Spec. Top.* **2007**, *141*, 153−160.
(40) van Zanten, J. H.; Wallace, W. E.; Wu, W. l. *Phys. Rev. E* **1996**, *53*, R2053.
(41) Grohens, Y.; Sacristan, J.; Hamon, L.; Reinecke, H.; Mijangos, C.; Guenet, J. M. *Polymer* **2001**, *42*, 6419−6423.
(42) Napolitano, S.; Prevosto, D.; Lucchesi, M.; Pingue, P.; D'Acunto, M.; Rolla, P. *Langmuir* **2007**, *23*, 2103−2109.
(43) Serghei, A.; Tress, M.; Kremer, F. *Macromolecules* **2006**, *39*, 9385−9387.
(44) Napolitano, S.; Lupascu, V.; Wübbenhorst, M. *Macromolecules* **2008**, *41*, 1061−1063.
(45) Mundra, M. K.; Ellison, C. J.; Behling, R. E.; Torkelson, J. M. *Polymer* **2006**, *47*, 7747−7759.
(46) Yang, Z.; Fujii, Y.; Lee, F. K.; Lam, C.-H.; Tsui, O. K. C. *Science* **2010**, *328*, 1676−1679.
(47) Fryer, D. S.; Peters, R. D.; Kim, E. J.; Tomaszewski, J. E.; de Pablo, J. J.; Nealey, P. F.; White, C. C.; Wu, W.-l. *Macromolecules* **2001**, *34*, 5627−5634.
(48) Serghei, A.; Kremer, F. *Macromol. Chem. Phys.* **2008**, *209*, 810−817.
(49) Napolitano, S.; Wübbenhorst, M. *Nature Commun.* **2011**, *2*, 260.
(50) Tsui, O. K. C.; Russell, T. P.; Hawker, C. J. *Macromolecules* **2001**, *34*, 5535−5539.
(51) Grohens, Y.; Hamon, L.; Reiter, G.; Soldera, A.; Holl, Y. *Eur. Phys. J. E* **2002**, *8*, 217−224.
(52) Pham, J. Q.; Green, P. F. *J. Chem. Phys.* **2002**, *116*, 5801.
(53) Soles, C. L.; Douglas, J. F.; Jones, R. L.; Wu, W.-l. *Macromolecules* **2004**, *37*, 2901−2908.
(54) Soles, C. L.; Douglas, J. F.; Wu, W.-l.; Peng, H.; Gidley, D. W. *Macromolecules* **2004**, *37*, 2890−2900.
(55) Torkelson, J. M.; Priestley, R. D.; Rittigstein, P.; Mundra, M. K.; Roth, C. B. *AIP Conf. Proc.* **2008**, *982*, 192−195.
(56) Reiter, G.; Hamieh, M.; Damman, P.; Sclavons, S.; Gabriele, S.; Vilmin, T.; Raphael, E. *Nature Mater.* **2005**, *4*, 754−758.
(57) Strunskus, T.; Zaporojtchenko, V.; Behnke, K.; v. Bechtolsheim, C.; Faupel, F. *Adv. Eng. Mater.* **2000**, *2*, 489−492.
(58) Mathieu, H. J.; Datta, M.; Landolt, D. *J. Vac. Sci. Technol., A* **1985**, *3*, 331.
(59) Kremer, F.; Schönhals, A. In *Broadband Dielectric Measurement Techniques in Broadband Dielectric Spectroscopy*; Kremer, F., Schönhals, A., Eds.; Springer: Berlin, 2002; p 35.
(60) Schartel, B.; Wendorff, J. H. *Polymer* **1995**, *36*, 899−904.
(61) Alegría, A.; Mitxelena, O.; Colmenero, J. *Macromolecules* **2006**, *39*, 2691−2699.
(62) Arrese-Igor, S.; Mitxelena, O.; Arbe, A.; Alegría, A.; Colmenero, J.; Frick, B. *Phys. Rev. E* **2008**, *78*, 021801.
(63) Schaefer, J.; Stejskal, E. O.; Buchdahl, R. *Macromolecules* **1977**, *10*, 384−405.
(64) Floudas, G.; Higgins, J. S.; Kremer, F.; Fischer, E. W. *Macromolecules* **1992**, *25*, 4955−4961.
(65) Havriliak, S.; Negami, S. *J. Polym. Sci., Part C: Polym. Symp.* **1966**, *14*, 99−117.
(66) Schönhals, A.; Kremer, F. In *Analysis of Dielectric Spectra in Broadband Dielectric Spectroscopy*; Kremer, F., Schönhals, A., Eds.; Springer: Berlin, 2002; p 59.
(67) (a) Vogel, H. *Phys. Z.* **1921**, *22*, 645. (b) Fulcher, G. S. *J. Am. Ceram. Soc.* **1925**, *8*, 339. (c) Tammann, G.; Hesse, W. *Z. Anorg. Allg. Chem.* **1926**, *156*, 245.
(68) Angell, C. A. *J. Non-Cryst. Solids* **1991**, *131*−*133* (Part 1), 13−31.
(69) Angell, C. A. *J. Res. Natl. Inst. Stand. Technol.* **1997**, *102*, 171−185.
(70) Hartmann, L.; Fukao, K.; Kremer, F. In *Molecular Dynamics in Thin Polymer Films in Broadband Dielectric Spectroscopy*; Kremer, F., Schönhals, A., Eds.; Springer: Berlin, 2002; p 433.
(71) Kremer, F.; Schönhals, A. In *The Scaling of the Dynamics of Glasses and Supercooled Liquids Spectra in Broadband Dielectric Spectroscopy*; Kremer, F., Schönhals, A., Eds.; Springer: Berlin, 2002; p 99.
(72) Kremer, F.; Schönhals, A. In *Broadband Dielectric Measurement Techniques in Broadband Dielectric Spectroscopy*; Kremer, F., Schönhals, A., Eds.; Springer: Berlin, 2002; p 10.
(73) Rotella, C.; Wübbenhorst, M.; Napolitano, S. *Soft Matter* **2011**, *7*, 5260−5266.
(74) Napolitano, S.; Pilleri, A.; Rolla, P.; Wübbenhorst, M. *ACS Nano* **2010**, *2*, 841−848.
(75) Napolitano, S.; Wübbenhorst, M. *J. Phys. Chem. B* **2007**, *111*, 9197−9199.
(76) Peter, S.; Napolitano, S.; Meyer, H.; Wübbenhorst, M.; Baschnagel, J. *Macromolecules* **2008**, *41*, 7729−7743.
(77) Kremer, F.; Schönhals, A. In *The Scaling of the Dynamics of Glasses and Supercooled Liquids Spectra in Broadband Dielectric Spectroscopy*; Kremer, F., Schönhals, A., Eds.; Springer: Berlin, 2002; p 99.
(78) Baschnagel, J.; Binder, K. *Macromolecules* **1995**, *28*, 6808−6818.
(79) Lipson, J. E. G.; Milner, S. T. *Eur. Phys. J. B* **2009**, *72*, 133−137.
(80) Milner, S. T.; Lipson, J. E. G. *Macromolecules* **2010**, *43*, 9865−9873.
(81) Napolitano, S.; Rotella, C.; Wübbenhorst, M. *Macrom. Rapid Commun.* **2011**, *32*, 844−848.
(82) Napolitano, S.; Wübbenhorst, M. *Polymer* **2010**, *51*, 5309−5312.

(83) Van Oss, C. J.; Chaudhury, M. K.; Good, R. J. *Chem. Rev.* **1988**, *88*, 927−941.
(84) Lee, L.-H. *Langmuir* **1996**, *12*, 1681−1687.
(85) Good, R. J.; Girifalco, L. A. *J. Phys. Chem.* **1960**, *64*, 561−565.
(86) Massoro, C.; Le, Q. T.; Pireaux, J. J. *Surf. Interface Anal.* **1994**, *21*, 425−429.
(87) An alternative explanation to the trend in Figure 9 is the effect of the nonzero dielectric dissipation of the thin layer of oxide present on the surface of the metallic electrodes. The sum of the contribution of the inorganic layer, dielectric constant >9 and almost constant loss $\sim 10^{-3}$, to the capacitance of the polymer is more relevant in the frequency region where no molecular relaxation is active. However, considering the large value of the residual dielectric strength, the related increase in dielectric loss in between the structural relaxation and the secondary process should be observed at thicknesses 1 order of magnitude smaller.
(88) Donth, E. In *The Glass Transition: Relaxation Dynamics in Liquids and Disordered Materials*; Donth, E., Ed.; Springer: Berlin, 2001; p 269.
(89) Wübbenhorst, M.; Murray, C. A.; Forrest, J. A.; Dutcher, J. R. *Proc. 11th Int. Symp. Electrets* **2002**, 401.